Comprehensive *ab initio* study of properties of monovacancies and antisites in 4H-SiC

2001 J. Phys.: Condens. Matter 13 6203

(http://iopscience.iop.org/0953-8984/13/28/305)

INSTITUTE OF PHYSICS PUBLISHING JOURNAL OF PHYSICS: CONDENSED MATTER

J. Phys.: Condens. Matter **13** (2001) 6203–6231 PII: S0953-8984(01)24214-3

Comprehensive *ab initio* study of properties of monovacancies and antisites in 4H-SiC

L Torpo, M Marlo, T E M Staab[1] and R M Nieminen

Helsinki University of Technology, Laboratory of Physics, PO Box 1100, FIN-02015 HUT, Finland

E-mail: leena.torpo@hut.fi (L Torpo) and tst@fyslab.hut.fi (T E M Staab)

Received 24 April 2001
Published 29 June 2001
Online at stacks.iop.org/JPhysCM/13/6203

Abstract

We present results of *ab initio* calculations for the electronic and atomic structures of monovacancies and antisite defects in 4H-SiC in all possible charge states. The calculations make use of a plane-wave pseudopotential method based on density-functional theory and the local spin-density approximation. Formation energies, ionization levels, and local geometries of the relaxed structures are reported for defects at all possible cubic and hexagonal lattice sites. To correct for the electrostatic interaction between charged supercells, we use a Madelung-type correction for the formation energies, leading to good agreement with experimentally observed ionization levels. Our calculations indicate no negative-U behaviour for carbon vacancies. Hence, the singly positive charge state of the carbon vacancy V_C^+ is stable, as recently found in experiments. The silicon antisite Si_C^+ is found to be stable at low values of electron chemical potential—again in agreement with experiment.

1. Introduction

Silicon carbide has excellent mechanical stability. It can withstand chemically hostile environments, high temperatures, high electric fields, and high frequencies. Due to its various superior characteristics, SiC has great potential for various demanding electronic applications. The main obstacle to SiC becoming a widespread semiconductor material is the problems arising from high-quality large-area crystal growth. Furthermore, semiconductor processing requires controlled incorporation of dopants, whereas the presence of other defects is not generally favourable. In order to tailor the properties of a semiconductor in a desired way, the electronic structure and the stability of both the wanted and unwanted defects must be well understood.

[1] Present address: Rheinische Friedrich-Wilhelms Universität Bonn, Institut für Strahlen- und Kernphysik, Nußallee 12-16, D-53115 Bonn, Germany.

0953-8984/01/286203+29$30.00

SiC is an interesting material for technological applications; the problems arising in growth of the material stem from the fact that it is also one of the rare materials which can exist in several crystalline modifications—so-called *polytypes*. All the polytypes of SiC can be described on the basis of a hexagonal lattice where the different modifications arise from the different stacking sequences of carbon and silicon planes [1]. One of the problems in growth arises from the difficulty of retaining one specific polytype. Apart from two polytypes, all other SiC structures contain both hexagonal and cubic lattice sites. 3C-SiC, i.e. the zinc-blende structure, has only cubic lattice sites while 2H-SiC, the wurtzite structure, has only hexagonal lattice sites. The properties of different SiC polytypes can be quite different. For example, the band gap of 3C is 2.39 eV while for 2H it is 3.33 eV. The technologically most interesting polytypes 4H- and 6H-SiC are mixtures of wurtzite and zinc-blende crystal structures, which results in there being two inequivalent lattice sites for both carbon and silicon atoms.

Native point defects in a SiC crystal include vacancies, antisites, and interstitials. These simple, isolated point defects may be produced experimentally by electron or proton irradiation at low temperatures. Raising the sample temperature during annealing treatments makes these defects either unstable or mobile. One example for unstable point defects has been considered in [2] in the form $V_{Si} \rightarrow C_{Si}V_C$, i.e. the conversion of a silicon vacancy to a carbon antisite–carbon vacancy pair. While mobile primary defects also give rise to various defect complexes, in this study we concentrate on investigating the simplest point defects: vacancies and antisites.

Experimentally, point-defect-related centres in SiC are observed after irradiation treatment or as grown-in defects by means of photoluminescence (PL) [3–7], optically detected magnetic resonance (ODMR) and electron paramagnetic resonance spectroscopy (EPR) [3, 4, 8–12], electron–nuclear double resonance (ENDOR) [13], and by positron annihilation spectroscopy (PAS) [14–18]. Also various capacitance transient techniques such as deep-level transient spectroscopy (DLTS) have been used in SiC defect studies [19–22]. For a comparison with experimental results we will concentrate on the as-irradiated state after electron or proton irradiation, since thus mainly simple, isolated point defects are created.

In spite of the recent progress in experimental SiC characterization, the atomistic identification of its defects is still limited. So far, among point defects only the silicon monovacancy in its singly negative charge state has been conclusively identified from experiments [13]. On the other hand, there are numerous tentative assignments for other defects in SiC. Promising results have been obtained, from among others EPR spectroscopy [11] and positron annihilation measurements, where already the silicon antisite [11] and both the silicon and carbon monovacancy, and the Si–C divacancy, appear to have been observed [14, 18, 23]. But the defect identification is hampered by the obvious lack of accurate theoretical data. Theoretical and experimental studies of electronic, structural, and optical properties must be correlated for an unambiguous identification of point defects.

In the theoretical literature, point defects in SiC were studied more than a decade ago, first using a tight-binding approach [24, 25], but also employing pseudopotential calculations without full ionic relaxations and using only a comparatively small supercell [26]. An all-electron LMTO-ASA study for the unrelaxed V_{Si} was carried out later [13]. Recently, accurate pseudopotential calculations with full ionic relaxations employing larger supercells have appeared [27–31]. Nevertheless, the present understanding of point defects in SiC is still far from complete.

Usually, data stemming from calculations performed by different research groups suffer from the fact that they are not comparable to a high accuracy due to the slightly different approximations used (pseudopotentials, plane-wave cut-off energies, Brillouin-zone sampling, etc). In this paper, we present a comprehensive *ab initio* study of the physical properties of all simple point defects (monovacancies and antisites) in 4H-SiC. This gives us the unique

possibility of comparing even small differences. The defects at cubic and hexagonal lattice sites are considered separately in our calculations. We discuss the error margins of calculated results in the framework of the plane-wave pseudopotential (PWPP) method, and try to evaluate to what extent the calculated and experimental results are comparable.

To compare our results to those from experimental magnetic resonance methods (EPR, ODMR, ENDOR), we determine for all defects in all their possible charge states the symmetries and the total spin. Furthermore, we determine the ionization levels and compare our results to experimental data from PL, DLTS, and PAS. We make an attempt to present the calculated properties such that they can be compared to other calculations or to experimental observations in a straightforward manner. Therefore, the data are presented without any correction for the well known band-gap problem arising from the local density approximation. Rather, we indicate the Kohn–Sham band edge below the experimental conduction band. We do correct for the electrostatic interaction between charged supercells by employing a Madelung-type correction for the formation energies [32]. However, from the point of view of density-functional theory (DFT) alone we do not claim that the effect of the Madelung correction on the ionization levels is fully understood and absolutely correct. The use of the macroscopic dielectric constant may overestimate the correction. Nevertheless, this procedure will be shown to lead to good agreement with experimentally observed ionization levels.

The outline of the article is as follows. In section 2, we describe the computational PWPP scheme used in detail. In section 3, we present the results for the neutral defects, while section 4 contains the results for the charged defects: the formation energy curves, the positions of the ionization levels, and the atomic relaxations around the defects. Finally, we discuss in section 5 the calculated results together with experimental observations and recent theoretical calculations for point defects in SiC.

2. Method

2.1. Basic computational methods

We use a plane-wave pseudopotential method [33, 34], where the exchange–correlation functional of the many-body electron–electron interaction is described within the local spin-density approximation (LSDA) [33–35]. In order to describe the valence electrons, plane-wave basis functions are used, while the core electrons are described by pseudopotentials. For the Si ions we use the standard norm-conserving Bachelet–Hamann–Schlüter (BHS) pseudopotentials [36]. In order to reduce the number of plane waves needed to describe electron wave functions, we employ for the C ion the Vanderbilt non-norm-conserving ultrasoft pseudopotential [37, 38] with a core radius of 1.3 au.

In our defect calculations, all of the ions in the supercell have been allowed to relax without any symmetry constraints using the Broyden–Fletcher–Goldfarb–Shanno (BFGS) algorithm (see e.g. [39]) in order to attain the minimum-energy configuration. The initial atomic configurations have been randomized from the ideal structure to remove any spurious symmetries. For the electronic structure minimization, we employ damped second-order dynamics [40] combined with the Williams–Soler algorithm [41]. All calculations have been performed in a massively parallel CRAY-T3E system using the carefully optimized FINGER (**Fin**nish **g**eneral **e**lectron **r**elaxator) code [42].

The convergences of the cohesive energy, lattice constant, bulk modulus, and its first pressure derivative in 3C-SiC are studied as functions of the kinetic energy cut-off. The structural parameters are well converged with plane-wave kinetic energies of 20 Ryd (see figure 1). Hence, we use this PW cut-off in the following work.

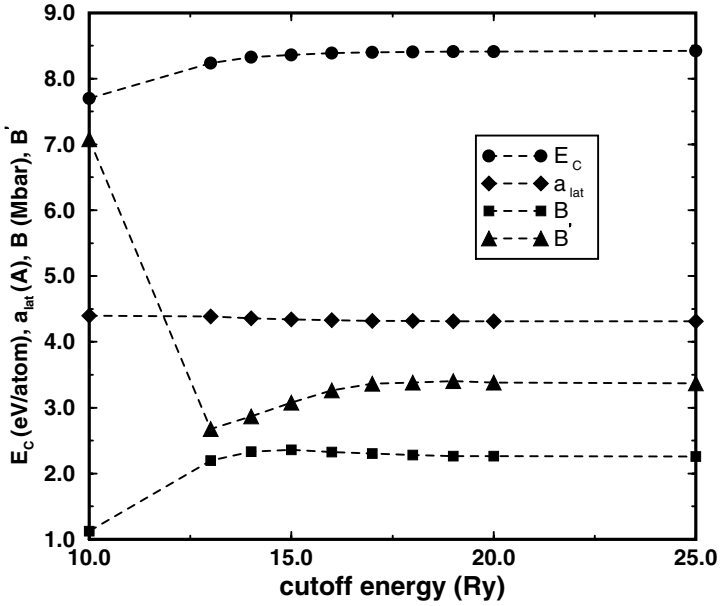

Figure 1. Convergence of structural parameters as functions of the plane wave cut-off for 3C-SiC: cohesive energy E_{C}, lattice constant a_{lat}, bulk modulus B, and first pressure derivative B'.

The structural properties of 4H-, 2H-, and 3C-SiC obtained with a kinetic energy cut-off of 25 Ryd are presented in table 1. In 3C-SiC, all calculated and referenced values are obtained by a fit to the Murnaghan equation of state [43]. Our results are compared with previous pseudopotential calculations for structural parameters for different polytypes and experiments. We chose reference [1], because in this study a code (FHI93) similar to FINGER has been used. The differences between the results should arise only from different soft pseudopotentials used to model the carbon ion.

Table 1. Calculated cubic and hexagonal lattice constants given in Å: $a_{3\mathrm{C}}$, $a_{2\mathrm{H}}$, $c_{2\mathrm{H}}$, $a_{4\mathrm{H}}$, and $c_{4\mathrm{H}}$. For 3C we give the bulk modulus B in Mbar and the first pressure derivative B'. For comparison, the corresponding values from previous DFT-LDA calculations and from experiments are presented. (For 3C, the hexagonal lattice constant is obtained by dividing the cubic lattice constant by $\sqrt{3}$).

	$a_{3\mathrm{C}}$	$a_{2\mathrm{H}}$	$c_{2\mathrm{H}}$	c/a (2H)	$a_{4\mathrm{H}}$	$c_{4\mathrm{H}}$	c/a (4H)	B(3C)	B'(3C)
[a]	4.291	3.031	4.960	1.637	3.032	9.928	3.274	2.22	334
[b]	4.305	3.045	4.993	1.640	3.039	9.978	3.283	2.26	337
[c]	4.360	3.076	5.048	1.641	3.078	10.086	3.277	2.24	390

[a] *Ab initio* result from reference [1].
[b] This work.
[c] Experimental result: see volumes III/22a and III/17a of [44].

The (smallest) unit cell of the 4H structure is described by hexagonal lattice vectors and eight basis atoms. In this case the unit cell is elongated along the c-axis (ratio $c/a = 1.63$). However, it is possible to construct a perfect 4H-SiC lattice using rectangular lattice vectors as well. In our defect calculations we use such a rectangular supercell, which is as close to cubic as possible. This is done to minimize the defect–defect interactions by separating defects in the periodic superlattice as much as possible. Testing many other cell sizes and shapes as well

as different k-point samplings, this choice turns out to be computationally the most efficient, because we obtain for the rectangular (nearly cubic) shaped cell well converged results using for the Brillouin-zone sampling only the Γ point. Hence, we performed all the defect calculations in the LSDA scheme using the Γ point in a 128-atom supercell. The rectangular basis vectors given in atomic units are $a_x = 19.890$, $a_y = 22.967$, and $a_z = 18.860$.

2.2. Total energies and defect formation energies in supercell calculations

In order to obtain information about the equilibrium concentrations and the ionization levels of native defects, we calculate the formation energies for all defects studied in all their possible charged states.

The energy required to form a defect in an otherwise perfect crystal is the free energy of formation ($\Omega_F = E_F - TS$). The temperature-dependent part of Ω_F describes the entropy effects of ionic vibrations (phonons), which are non-trivial to calculate. Therefore, the contribution from the phonon entropy is often ignored. At low temperatures the free energy of formation Ω_F and, thus, the concentrations of defects in thermodynamic equilibrium are largely determined by the formation energy E_F, with only minor contributions arising from the phonon entropy. However, at elevated temperatures, the anharmonic effects in the entropy term may have a significant influence on Ω_F. These are, however, beyond the scope of the present work.

The formation energy E_F can be evaluated directly from electronic structure calculations. We determine the formation energies using the standard formalism of Zhang and Northrup [45], where the formation energy E_F of a defect in the charge state q is expressed as follows:

$$E_F = E_{tot}(q) + q(E_V + \mu_e) - \sum_s n_s \mu_s. \tag{1}$$

Here, μ_e is the electron chemical potential (often also denoted as E_F for the Fermi level)[2]. $E_{tot}(q)$ is the calculated total energy of the supercell containing n_C carbon and n_{Si} silicon atoms and the defect. Additionally, it may have an excess charge q. If the defect binds extra charge, this has to be transferred from a reservoir to the level of the electron chemical potential (μ_e), measured relative to the valence band maximum (E_V). The sum runs over the atomic species involved and describes the energy which n_C carbon and n_{Si} silicon atoms would have in the ideal SiC crystal.

Unfortunately, the exact values of the chemical potentials of the constituents (μ_{Si}, μ_C) of the compound crystal cannot be uniquely determined. We can only state that

$$\mu_{SiC} = \mu_{Si} + \mu_C \tag{2}$$

where μ_{SiC} is the energy per Si–C pair in the SiC crystal. In addition, the chemical potentials of atomic constituents in SiC cannot exceed their elemental bulk values ($\mu_{Si} \leqslant \mu_{Si}^{bulk}$, $\mu_C \leqslant \mu_C^{bulk}$).

If we define the chemical potential difference

$$\Delta\mu = (\mu_{Si} - \mu_C) - \left(\mu_{Si}^{bulk} - \mu_C^{bulk}\right) \tag{3}$$

and note that under extremely Si-rich or C-rich preparation conditions the chemical potentials of the constituents approach their corresponding bulk values, we can see that $\Delta\mu$ is limited by the heat of formation (ΔH) of the SiC crystal:

$$\Delta H = \mu_{Si}^{bulk} + \mu_C^{bulk} - \mu_{SiC}^{bulk}. \tag{4}$$

[2] We prefer to use the symbol μ_e, since a semiconductor does not have a Fermi surface and, hence, the Fermi level is not properly defined.

In fact, $\Delta\mu$ can be related to the deviation from ideal stoichiometry. Hence, it can vary from $-\Delta H$ (C-rich) to ΔH (Si-rich). For 4H-SiC, we calculate the heat of formation to be 0.67 eV. Now the formation energy (equation (1)) can be rewritten using $\Delta\mu$:

$$E_{\mathrm{F}} = E_{\mathrm{tot}}(q) - \frac{1}{2}(n_{\mathrm{Si}} + n_{\mathrm{C}})\mu_{\mathrm{SiC}}^{\mathrm{bulk}} - \frac{1}{2}(n_{\mathrm{Si}} - n_{\mathrm{C}})\left(\mu_{\mathrm{Si}}^{\mathrm{bulk}} - \mu_{\mathrm{C}}^{\mathrm{bulk}}\right) + q E_{\mathrm{V}} + q\mu_{\mathrm{e}} - \frac{1}{2}(n_{\mathrm{Si}} - n_{\mathrm{C}})\Delta\mu. \tag{5}$$

We plot (figure 2; see section 4.1) the formation energies as functions of the electron chemical potential from the valence band maximum E_{V} to the value of the band gap (E_{gap}). The appropriate value for the chemical potential difference $\Delta\mu$ depends on the defect and defect formation processes.

The ionization level (q/q') of a given defect is the position of μ_{e} in the band gap where the most stable charge state changes from q to q'. Ionization levels can be obtained by solving the following equation for the value of the electron chemical potential μ_{e}:

$$E_{\mathrm{tot}}(q) + q(E_{\mathrm{V}} + \mu_{\mathrm{e}}) = E_{\mathrm{tot}}(q') + q'(E_{\mathrm{V}} + \mu_{\mathrm{e}}). \tag{6}$$

The computational DFT-LSDA method has some unresolved problems, which can have a significant influence on the ionization levels. The most important is the gap problem: in the electronic structure calculations the band gap is extracted from Kohn–Sham single-particle energy levels. Formally, these levels do not describe any physical quantity—only the total energy is well defined. Although Kohn–Sham eigenvalues sometimes agree quite nicely with the true quasiparticle band structure, the width of the band gap is always severely underestimated. We obtain for the energy gap of 3C- and 4H-SiC 1.24 and 2.6 eV, respectively, while the corresponding experimental values are 2.39 and 3.27 eV. Since defect states appear in the band gap, there can be problems in interpreting the actual positions of the ionization levels according to equation (6). In this work, the calculation of the ionization levels is based on the total energies. We will consistently report ionization levels measured from the valence band maximum (VBM). However, when plotting the formation energies, we indicate also the position of the LDA gap and leave it to the reader to measure the distance of an ionization level from the experimental conduction band minimum (CBM) or from the Kohn–Sham band edge.

Another possible source of error affecting the ionization levels arises from the charged supercells. Even though we use supercells that are as big as is computationally possible, the localized charge distribution with its neutralizing background around each defect interacts with neighbouring supercells due to the long-range nature of the Coulomb interaction. The electrostatic interaction between supercells gives rise to an error which scales with the charge squared (q^2) and depends inversely on the supercell dimension L. Due to the q^2-dependence, this error becomes significant for highly charged defects (± 2, ± 3, and ± 4). It is non-trivial to calculate the accurate correction: in order to roughly evaluate the error, we use the heuristic approach introduced by Makov and Payne [32]. Using this formalism, the electrostatic interaction energy between charged supercells is

$$E = E_0 - \frac{q^2\alpha}{2L\epsilon} - \frac{2\pi q Q}{3L^3\epsilon} + \mathrm{O}(L^{-5}) \tag{7}$$

where E_0 is the total energy obtained from the calculations, q is the charge of the supercell, Q its quadrupole moment, α the Madelung constant, ϵ the static dielectric constant, and L the size of the supercell used. The Madelung constant used here is $\alpha = 1.41865$ (estimated for the rectangular cell containing 128 atoms; the cell size is 19.89 au) and for ϵ we take the experimental value of 6.7. For 4H-SiC we obtain corrections for $q = \pm 1$ of $\approx$0.19 eV, while for $q = \pm 2$ they are $\approx$0.75 eV. However, by calculating only the first term, we may

overestimate the error (the second term is about one third of the value of the first correction term [46]. Hence, we should also be careful in interpreting the results after the correction. In order to compare the results both with other calculations and with the experiments and discuss them, we present the data with and without the Medelung correction.

3. Neutral defects

The calculated formation energies for neutral antisites and vacancies are presented in table 2. The results are given for both cubic and hexagonal sites in 4H-SiC. As discussed in the previous section, there is no unique way to determine the formation energy, since it depends on the chemical potentials of the atoms, i.e. on the stoichiometry of the compound. This implies that the formation energy depends on the conditions under which the defects are formed (growth, processing, and annealing). Hence, the chemical potential difference can have different values varying over a range of 1.33 eV for antisites and 0.67 eV for vacancies from Si- to C-rich. In table 2, the formation energy values are given for Si-rich ($\Delta\mu = \Delta H$), stoichiometric ($\Delta\mu = 0$), and C-rich ($\Delta\mu = -\Delta H$) material.

Table 2. Formation energies (in eV) of neutral point defects in 4H-SiC. The results are for antisites as well as for silicon and carbon monovacancies. The values of the formation energy are given for stoichiometric ($\Delta\mu = 0$) as well as for Si- and C-rich material. The calculations are made for both cubic and hexagonal lattice sites, as indicated by the superscripts 'cub' for the cubic site and 'hex' for the hexagonal atom site.

Defect	Si-rich: $\Delta\mu = \Delta H$	Stoichiometric: $\Delta\mu = 0$	C-rich: $\Delta\mu = -\Delta H$
Silicon antisites			
Si_C^{cub}	3.62	4.29	4.95
Si_C^{hex}	3.58	4.25	4.92
Carbon antisites			
C_{Si}^{cub}	4.19	3.52	2.85
C_{Si}^{hex}	4.24	3.57	2.90
Silicon vacancies			
$V_{Si}^{cub}(S = 0)$	8.70	8.37	8.03
$(S = 1)$	8.37	8.03	7.70
$V_{Si}^{hex}(S = 0)$	8.60	8.26	7.93
$(S = 1)$	8.40	8.06	7.73
Carbon vacancies			
V_C^{cub}	3.74	4.07	4.41
V_C^{hex}	3.82	4.21	4.49

For stoichiometric material the carbon antisite C_{Si}^{cub} at the cubic lattice site has the lowest formation energy: 3.52 eV. But the carbon vacancy V_C^{cub} and the silicon antisite Si_C^{hex} also have low formation energies of 4.07 eV and 4.25 eV, respectively, while the silicon vacancy has a much higher formation energy of about 8 eV. Hence, in Si-rich material, Si_C^{hex} and V_C^{cub} are likely to dominate according to their formation energies of 3.58 and 3.74 eV, respectively. In C-rich material, the clearly most dominant defect will be the carbon antisite, since the formation energy of C_{Si}^{cub} takes values as low as 2.85 eV.

The formation energy values differ between defects in cubic and hexagonal atom sites only by a comparatively small amount (0.03–0.14 eV)—depending on the defect. We find

generally that the energy required to form a defect on a cubic site is slightly lower than the corresponding one for the hexagonal lattice site. However, the difference is so small that it is not expected to influence the defect concentrations significantly.

Our results for monovacancies are in accordance with the PWPP results reported recently by Zywietz *et al* in reference [27]. In section 5, we will discuss our results for 4H-SiC together with the results obtained recently for other polytypes (references [26–30]).

4. Charged defects

In this section, we present results for monovacancies and antisite defects in all their relevant charge states. The results provide information on ionization levels, stabilities of different charge states, and point group symmetries of the defects. We also discuss how the lattice site of 4H-SiC (cubic or hexagonal) modifies defect properties such as atomic relaxations around a given defect.

Considering charged defects, their formation energy depends on the position of the electron chemical potential according to equation (1) or (5). When the electron chemical potential is low (Fermi level below the mid-gap—close to the valence band), positive charge states are favoured. At high values of the electron chemical potential (Fermi level above the mid-gap—close to the conduction band), defects are able to bind extra electrons and negative charge states are more favourable. The ionization levels are defined as those values of the electron chemical potential (μ_e) where the formation energy lines of two stable charge states intersect. In all the following figures, the formation energies arising from equation (5) are plotted as functions of the electron chemical potential μ_e for all charge states (straight lines). Additionally, we assume that defects are formed under stoichiometric conditions ($\Delta\mu = 0$). As explained in section 2, we present the data for the charged formation energies with and without the Madelung correction.

4.1. Silicon vacancy—ionization levels

For 4H-SiC we find several stable charge states, ranging from 2+ to 2−. Although they are likely to be unphysical, we have also calculated results for the highly negative charge states (3− and 4−). In figure 2 the formation energy for the silicon vacancy at the cubic and hexagonal lattice sites is shown as a function of the electron chemical potential. Panels (a) and (b) show results without the Madelung correction, while in panels (c) and (d) the Madelung correction is applied to correct the formation energies of charged defects.

The ionization levels of V_{Si} calculated from the total energies are also shown for both vacancy sites in table 3, while the levels for 3− and 4− are shown in table 4. The results in table 3 are compared with results obtained for other polytypes (2H and 3C) in reference [30], as well as to previous results for 4H-SiC [27]. The cited values for negative charge states in 4H-SiC taken from reference [27] are given in brackets, since they cannot be directly compared with our results. As explained in section 2, these levels are calculated from the conduction band minimum, and our results from the valence band maximum. However, the comparison can be made, provided that the gap difference $E_{EXP} - E_{LDA} \sim 1$ eV is added to our results for the levels $0/1-$ and $0/2-$.

Let us first discuss the results without the Madelung correction (figures 2(a), 2(b)). For very small values of the electron chemical potential (heavily p-type material) V_{Si} is stable in the charge state 2+. As the value of the electron chemical potential sweeps through the band gap, the vacancy can bind at least four additional electrons (corresponding to a charge state 2−), and theoretically, even more (corresponding to a charge state 4−). Compared to those for other point defects, the formation energy for the neutral vacancy V_{Si} in SiC is very high,

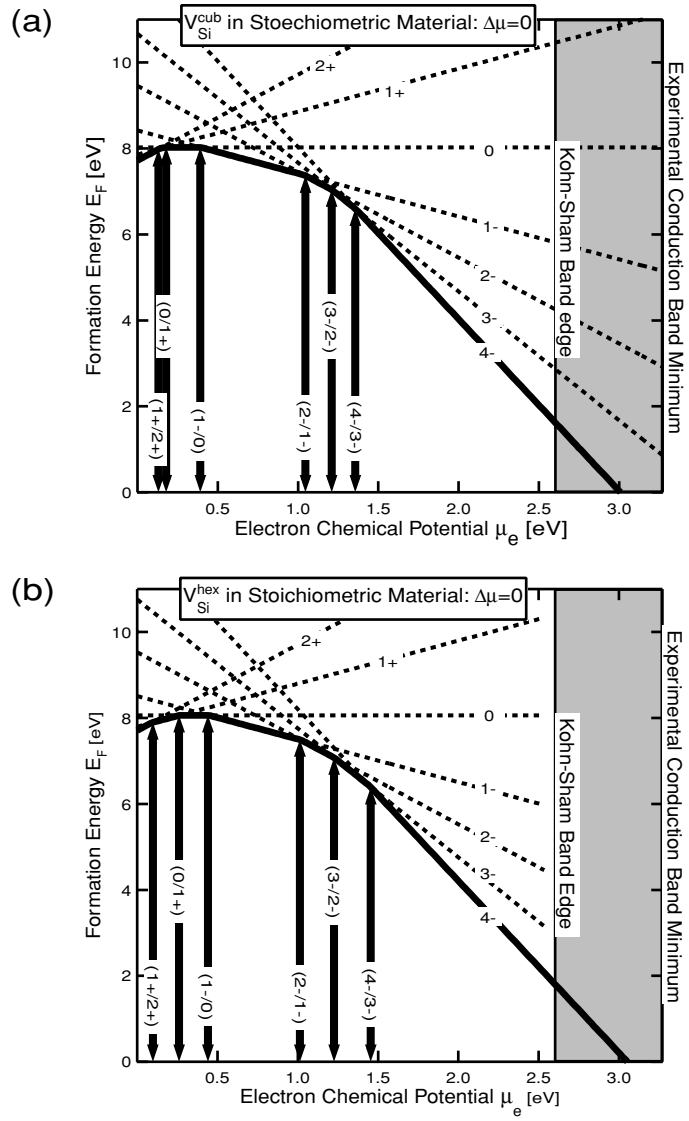

Figure 2. The silicon monovacancy at cubic ((a) and (c)) and hexagonal ((b) and (d)) lattice sites for stoichiometric material. Panels (a) and (b) ignore the Madelung correction, while panels (c) and (d) include it. Formation energies for different charge states (dashed lines), with each charge state indicated, are given. The thick solid line corresponds to the lowest formation energy as a function of the electron chemical potential. The ionization levels (indicated by arrows) are at the intersections of the dashed lines. Note that the highly negative charge states are shifted close to or into the conduction band when applying the Madelung correction.

∼8 eV. However, since V_{Si} in 4H-SiC can carry a charge from 2+ to 2−, its formation energy depends strongly on the value of the electron chemical potential. In particular, in C-rich SiC the formation energy of V_{Si}^{2-} may become as low as ∼4 eV (see figure 2), while for the positive charge state the formation energy remains relatively high, i.e. above 7 eV. For the silicon vacancy V_{Si} at both cubic and hexagonal lattice sites in 4H-SiC, we see that the lowest ionization level (2+/1+) is only 0.1 eV above the valence band maximum, while

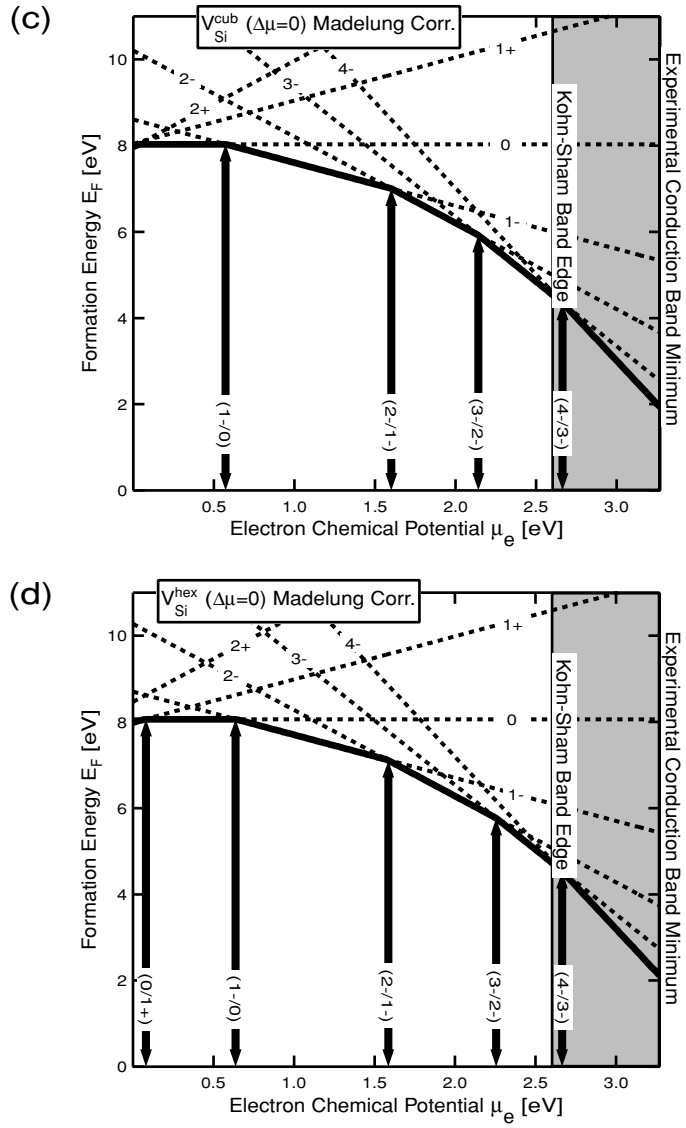

Figure 2. *Continued*

even the highly charged states are situated nearly all below the mid-gap. This seems to be unphysical.

When the Madelung correction is taken into account, the silicon vacancy does not stabilize in the charge state 2+ any longer (see figures 2(c), 2(d)). Additionally, only for the hexagonal site is the level (1+/0) found just above the VBM (see table 3). The Madelung correction also affects the negative charge states. Hence, the corresponding ionization levels are found deeper in the band gap: the level $(0/1-)$ is found at 0.6 eV above the VBM while $(1-/2-)$ is about 1 eV higher. It becomes doubtful whether the highest charge state $4-$ remains stable, since it moves above the Kohn–Sham band edge.

Table 3. Ionization levels from LSDA calculations for the relaxed silicon vacancy in 4H-SiC. The results are given in eV above the valence band maximum. For comparison, we also list results for other polytypes and from other calculations for 4H-SiC. The values in brackets are shifted as in Zywietz *et al* [27] and discussed in the text. For the values in the last three rows the Madelung correction has been applied.

	Ionization levels (eV above the VBM)			
Defect	2+/+	+/0	0/−	−/2−
4H: V_{Si}^{cub} [a]	0.14	0.18	0.38	1.04
4H: V_{Si}^{cub} [b]	0.06	0.20	(1.19)	(1.94)
4H:V_{Si}^{hex} [a]	0.09	0.27	0.45	1.02
4H: V_{Si}^{hex} [b]	0.08	0.31	(1.28)	(1.95)
3C: V_{Si} [c]	0.43	0.50	0.56 (1.56)	1.22 (2.22)
2H: V_{Si} [c]	0.05	0.13	0.32 (1.32)	0.91 (1.91)
Madelung correction applied				
4H: V_{Si}^{cub} [a]	−0.43	−0.02	0.57	1.60
4H: V_{Si}^{hex} [a]	−0.48	0.08	0.64	1.58
2H: V_{Si} [a]	−0.51	−0.06	0.51	1.47

[a] This work.
[b] Zywietz *et al* [27].
[c] Torpo *et al* [30].

Table 4. Ionization levels from LSDA calculations for highly negative charge states: for the relaxed silicon vacancy in 4H-SiC the results are given in eV above the valence band maximum. For comparison, we list also results for other polytypes (3C- and 2H-SiC) from reference [30]. The values in brackets are shifted as in reference [27]. For the values in the last three rows the Madelung correction has been applied.

	Ionization levels (eV above the VBM)	
Defect	2−/3−	3−/4−
4H: V_{Si}^{cub} [a]	1.21 (2.25)	1.36 (2.40)
4H: V_{Si}^{hex} [a]	1.23 (2.27)	1.45 (2.49)
3C: V_{Si} [c]	1.35 (2.35)	1.40 (2.40)
2H: V_{Si} [c]	1.04 (2.04)	1.24 (2.24)
Madelung correction applied		
4H: V_{Si}^{cub} [a]	2.14 (3.14)	2.67 (3.67)
4H: V_{Si}^{hex} [a]	2.26 (3.26)	2.66 (3.66)
2H: V_{Si} [c]	1.97 (2.97)	2.55 (3.55)

[a] This work.
[b] Zywietz *et al* [27].
[c] Torpo *et al* [30].

4.2. Silicon vacancy—spin effects

According to the simple one-electron model [47, 48], the electronic structure of a vacancy in a covalent solid is described by molecular orbitals constructed from four dangling bonds next to the vacancy. The defect molecular orbitals consist of the lowest a_1 one and a triply degenerate t_2 one, so a_1 can accommodate two electrons and t_2 six. However, the crystal can usually gain energy by relaxing atoms next to the vacancy. Lowering the symmetry destroys

the degeneracy of the t_2 orbital, provided that the energy gained by the overlapping dangling bonds overcomes the energy lost in distorting the lattice. This effect is called the *Jahn–Teller* distortion. The most prominent example is the silicon vacancy in Si bulk, which is subject to a strong Jahn–Teller distortion. It is well described by the single-electron picture [48, 49].

Although in some cases the ground state of the vacancy can be qualitatively described within a single-electron picture combined with lattice distortions, in most cases the complicated many-electron effects and the nature of surrounding crystal field dominate. For example, exchange effects of electrons in the degenerate t_2 orbital can be strong (electrons prefer parallel spins). For a vacancy system, which is not subject to a Jahn–Teller distortion, the exchange interactions can result in high-spin ground states.

The high-spin ground state for the vacancy in diamond has been confirmed experimentally [50]. Because the local atomic environments for the monovacancy in diamond and the silicon vacancy in silicon carbide are similar, it is natural to consider the possibility that vacancies can form high-spin states even in SiC. In fact, for SiC the high-spin ground state for the singly negative vacancy was also identified in both experiment and theory [13, 27, 30]. However, using multi-configurational self-consistent-field calculations it has been argued that for the ground state of the neutral silicon vacancy in 3C-SiC the spin singlet is about 0.1 eV more favourable than the spin-triplet state [51]. On the other hand, this calculation involved quite a small cluster where only the first-neighbour atoms were allowed to relax.

In order to study the total spin of the electronic structure of the silicon vacancy in 4H-SiC, spin-polarized (LSDA) calculations are performed both for high- and low-spin states considering all relevant charge states (0, 1−, 2−). By calculating total energies while fixing the total spin of the supercell to low- and high-spin values, we are able to compare the energies. The ground state is that one possessing the lowest energy. In terms of the simple molecular orbital model, the many-electron high-spin ground states result in the following filling of the a_1 and t_2 orbitals: $a_1^{\uparrow\downarrow}t_2^{\uparrow\uparrow}$, $a_1^{\uparrow\downarrow}t_2^{\uparrow\uparrow\uparrow}$, $a_1^{\uparrow\downarrow}t_2^{\uparrow\downarrow\uparrow\uparrow}$ for V_{Si}^{0}, V_{Si}^{1-}, V_{Si}^{2-}, respectively. The energy differences between low- and high-spin states, presented in table 5, indicate that high-spin states are the configurations with the lowest energy for all charge states of the silicon vacancy in 4H-SiC. The strongest exchange interaction, and the largest energy lowering in comparison to the low-spin state, is calculated for the singly negative charge state. In the following, we let the spins of the three gap states be parallel for the high-spin state $S = \frac{3}{2}$. For vacancies at hexagonal and cubic sites in 4H-SiC, we calculate an energy lowering compared to the low-spin state $S = \frac{1}{2}$ of $\Delta E = 530$ meV and $\Delta E = 440$ meV, respectively (see table 5). Also for the neutral and doubly negative charge states (V_{Si}^{0} and V_{Si}^{2-}) the high-spin state with $S = 1$ has a lower total energy (see table 5).

Furthermore, we find for V_{Si}^{1+} and V_{Si}^{3-}, which are low-spin ground-state defects, a prominent exchange interaction as well. This can be seen from table 5 as unexpected large differences in the total-energy values between spin-compensated (LDA) and spin-polarized (LSDA) calculations. In addition to the results of this work for 4H-SiC, we present in table 5 results previously obtained for 3C- and 2H-SiC in [30] as well as results from reference [27] for 4H-SiC. As mentioned before, strong exchange interactions are coupled to lattice relaxations presented for V_{Si} in the following section 4.3. Results concerning the high-spin states are further discussed in section 5. Spin effects for V_{C}^{0} in SiC have been reported and discussed in detail in references [27, 28, 30, 51].

Table 5. Spin-polarization effects in 4H-, 3C-, and 2H-SiC: considering different charge states of the silicon vacancy, the table shows the energy differences (in eV) $\Delta E = E^{\mathrm{LDA}} - E^{\mathrm{LSDA}}$ between spin-compensated (LDA) and the spin-polarized (LSDA) calculations. For 4H-SiC the values are given separately for cubic and hexagonal lattice sites. Within the LDA the spin state is always low, either $S = 0$ or $S = 1/2$, whereas within the LSDA the total spin S for each charge state corresponds to the ground-state spin configuration and is marked in the second column of the table. For comparison, we also list results for other polytypes and from other calculations for 4H-SiC.

	$\Delta E = E^{\mathrm{LDA}} - E^{\mathrm{LSDA}}$ (eV)				
Charge state:	1+	0	1−	2−	3−
LSDA; total spin S:	1/2	1	3/2	1	1/2
4H: V_{Si}^{cub} [a]	0.12	0.33	0.44	0.38	0.07
4H: V_{Si}^{cub} [b]	—	0.26	0.49	0.24	—
4H: V_{Si}^{hex} [a]	0.13	0.20	0.53	0.20	0.10
4H: V_{Si}^{hex} [b]	—	0.26	0.45	0.26	—
3C: V_{Si} [c]	0.08	0.38	0.58	0.42	0.24
2H: V_{Si} [c]	0.14	0.32	0.46	0.18	0.09

[a]This work.
[b]Zywietz *et al* [27].
[c]Torpo *et al* [30].

4.3. Silicon vacancy—relaxations

The relaxations around silicon vacancies at cubic and hexagonal lattice sites in 4H-SiC are given for different charge and spin states in table 6 and table 7, respectively. The four carbon atoms surrounding a Si vacancy are subject to a large net outward relaxation, reflected in an increase of the distances considered of about 10%. Alternatively, looking at the volume change of the tetrahedra defined by nearest-neighbour (NN) C atoms surrounding Si vacancies, those at cubic or hexagonal lattice sites show a volume increase from 25% to 36% and from 24% to 33%, respectively—depending on their charge state. Hence, the relaxation around Si vacancies at cubic lattice sites tends to be slightly larger (cf. tables 6 and 7).

Table 6. Relaxations around the cubic silicon vacancy V_{Si}^{cub} in 4H-SiC, given in % compared to the ideal tetrahedral distances between NN carbon atoms. The distances b_1–b_6 are labelled according to figure 3. The volume change is defined for the tetrahedra as $\Delta V = 100(V - V_0)/V_0$. The last column lists the symmetry groups for the defects.

		Tetrahedral distances (%) compared to ideal value							
Charge	Spin	b_1	b_2	b_3	b_4	b_5	b_6	ΔV	Symmetry
2+	0	+10.6	+10.5	+9.1	+10.5	+9.2	+9.1	+32.4	C_{3v}
1+	1/2	+10.1	+10.4	+9.0	+9.3	+9.1	+9.4	+31.4	C_{2v}
0	0	+7.2	+9.7	+8.4	+10.5	+9.4	+7.2	+28.4	$\sim C_{3v}$
0	1	+9.6	+9.0	+8.6	+9.7	+9.6	+9.0	+30.4	$\sim C_{3v}$
1−	1/2	+9.6	+9.5	+8.3	+9.8	+8.5	+8.5	—	C_{3v}
1−	3/2	+8.9	+8.8	+8.6	+9.1	+8.8	+8.8	+29.0	T_d
2−	0	+8.1	+8.1	+9.4	+11.0	+8.8	+8.7	+29.5	$\sim\sigma_{1v}$
2−	1	+9.6	+9.6	+9.0	+8.5	+9.9	+9.9	+30.9	C_{2v}
3−	1/2	+10.3	+9.1	+9.5	+10.0	+10.5	+10.8	+33.3	$\sim C_{2v}$
4−	0	+10.3	+10.3	+10.9	+10.6	+11.4	+11.4	+36.1	$\sim C_{3v}$

Table 7. Relaxations around the hexagonal silicon vacancy V_{Si}^{hex} in 4H-SiC given in % compared to the ideal tetrahedral distance between NN carbon atoms. The distances b_1–b_6 are labelled according to figure 3. The volume change is defined for the tetrahedra as $\Delta V = 100(V - V_0)/V_0$. The final column lists the symmetry groups for the defects.

		Tetrahedral distances (%) compared to ideal distance							
Charge	Spin	b_1	b_2	b_3	b_4	b_5	b_6	ΔV	Symmetry
2+	0	+9.8	+10.2	+9.9	+10.3	+10.0	+10.2	33.3	T_d
1+	1/2	+9.6	+10.1	+9.6	+9.7	+9.7	+10.0	32.1	C_{3v}/T_d
0	0	+8.9	+9.3	+8.1	+6.4	+9.7	+10.0	29.7	$\sim C_{2v}$
0	1	+9.0	+9.3	+8.5	+9.1	+9.1	+9.3	—	$\sim T_d$
1−	1/2	+8.6	+9.1	+7.6	+9.3	+7.4	+7.6	26.1	C_{3v}
1−	3/2	+7.8	+8.2	+7.9	+8.3	+7.9	+8.2	—	T_d
2−	0	+6.8	+9.8	+7.6	+7.0	+9.5	+7.3	26.6	$\sim D_{2d}$
2−	1	+8.1	+8.5	+7.9	+7.8	+8.3	+8.5	—	$\sim T_d/C_{3v}$
3−	1/2	+8.1	+8.8	+7.9	+8.0	+8.5	+8.5	27.1	$\sim C_{3v}$
4−	0	+8.2	+8.6	+8.3	+8.4	+8.2	+8.5	27.3	$\sim C_{3v}$

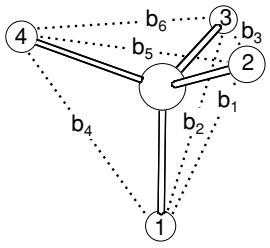

Figure 3. The distances of NN atoms around a vacancy in SiC making a tetrahedron. The labels b_1–b_6 are used in tables 6, 7, and 9 to indicate the relaxations.

The atomic geometries around Si vacancies, reported in tables 6 and 7, indicate that the symmetry is not much lowered around silicon vacancies, i.e. there are no prominent Jahn–Teller distortions, although the spin state is low. The point symmetry groups around vacancies are indicated in the last column in table 6 and in table 7. The point symmetry group for the silicon vacancy is generally T_d or close to that; less frequently a lower symmetry like $\sim C_{3v}$ is found.

In fact, the four carbon atoms, NN to V_{Si}, tend to change their bond angles with the three silicon atoms neighbouring them into a configuration where all four carbon atoms form sp^2-like bonds with their neighbouring silicon atoms—similar to graphite (see figure 4). This is in contrast to the Jahn–Teller-distorted Si vacancy in Si bulk, where the surrounding silicon atoms are likely to relax inwards, taking a configuration where two pairs of dangling bonds overlap.

4.4. Carbon vacancy—ionization levels

For the carbon vacancy in 4H-SiC, we find several stable charge states, ranging from 2+ to 2−, where the 2+, the neutral, and the 2− charge states are those lowest in energy and, hence, the most stable ones (see table 8 and figure 5).

Let us first look at the results without the Madelung correction applied: according to the calculations, on increasing the electron chemical potential for V_C^{2+}, two electrons become localized at the carbon vacancy, and thus the negative-U behaviour (2+/0) is observed. Hence, the ionization level (2+/1+) (cf. figure 5) should not be observable. A similar phenomenon

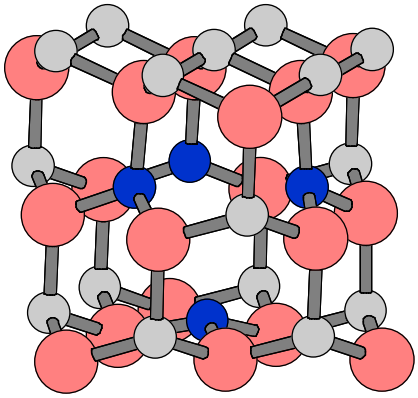

Figure 4. Relaxed atomic positions for the silicon monovacancy at the cubic lattice site in the singly negative charge state V_{Si}^{-}: the silicon atoms are the bigger, dark grey ones, while C atoms are light grey. The four small, black atoms (C) are the nearest neighbours to the missing Si atoms. Note the outward movement of NN C atoms leading to planar sp^2 bonds.

(This figure is in colour only in the electronic version)

occurs also between the charge states $(0/2-)$. Within the accuracy of LSDA-DFT, it is impossible to tell whether the singly positive or singly negative carbon vacancy V_C^{-} stabilizes for some value of the electron chemical potential.

For carbon vacancies at cubic lattice sites in 4H-SiC the ionization levels $(2+/1+)$ and $(1+/0)$ are not observed and the negative-*U* transition $(2+/0)$ is, according to our calculations, located at 1.57 eV above the VBM. The ionization levels $(0/1-)$ and $(1-/2-)$ are also not observed and the other negative-*U* transition $(0/2-)$ is located at 1.97 eV above the VBM (see figure 5(a) and table 8).

Table 8. V_C: ionization levels for the relaxed carbon vacancies in 4H-SiC. The results are from LSDA calculations given in eV above the valence band maximum. The upper part—without Madelung correction—leads to negative-*U* transitions, while in the lower part, when the Madelung correction is applied, the results indicate that the singly charged states (1+, 1−) stabilize as well.

	Ionization levels (eV above VBM)					
		Negative *U*			Negative *U*	
V_C	2+/1+	2+/0	1+/0	0/1−	0/2−	1−/2−
4H cubic [a]	(1.74)	**1.57**	(1.41)	(2.09)	**1.97**	(1.85)
4H hexagonal [b]	(1.68)		(1.37)	(2.74)		(2.45)
4H hexagonal [a]	(1.53)	**1.53**	(1.53)	(1.90)	**1.78**	(1.65)
4H hexagonal [b]	(1.68)		(1.44)	(2.71)		(2.42)
Madelung correction applied						
4H cubic [a]	1.18	—	1.22	2.28	—	2.41
4H hexagonal [a]	0.97	—	1.34	2.09	—	2.21

[a]This work.
[b]Zywietz *et al* [27].

For carbon vacancies at hexagonal lattice sites the charge states 2+, 0, and 2− stabilize at some values of the electron chemical potential. The singly positive charge state is nearly stable at 1.53 eV above the VBM. The respective ionization levels for $(2+/0)$ and $(0/2-)$ are

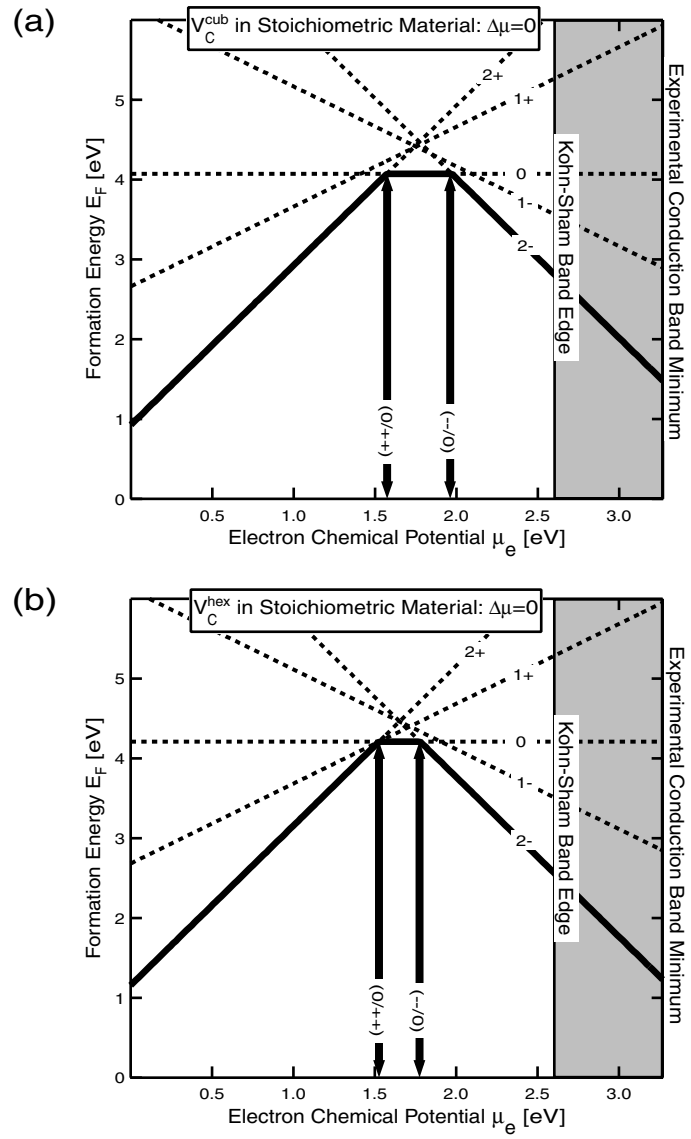

Figure 5. Carbon monovacancies at cubic ((a) and (c)) and hexagonal ((b) and (d)) lattice sites for stoichiometric material. Panels (a) and (b) ignore the Madelung correction, while panels (c) and (d) include it. Formation energies for different charge states (dashed lines), with each charge state indicated, are given. The thick solid line corresponds to the lowest formation energy as a function of the electron chemical potential. The ionization levels (indicated by arrows) are at the intersections of the dashed lines. Note that the negative-*U* behaviour vanishes when the Madelung correction is applied.

calculated for the hexagonal vacancy to be at 1.53 eV and 1.78 eV above the VBM (see figure 5(b), table 8, and reference [27]).

When the Madelung correction is applied, the formation energies change and V_C^{1+} and V_C^{1-} do stabilize (see figures 5(c) and 5(d)). The four ionization levels obtained are given in table 8. These results will be discussed in section 5 together with corresponding experimental data.

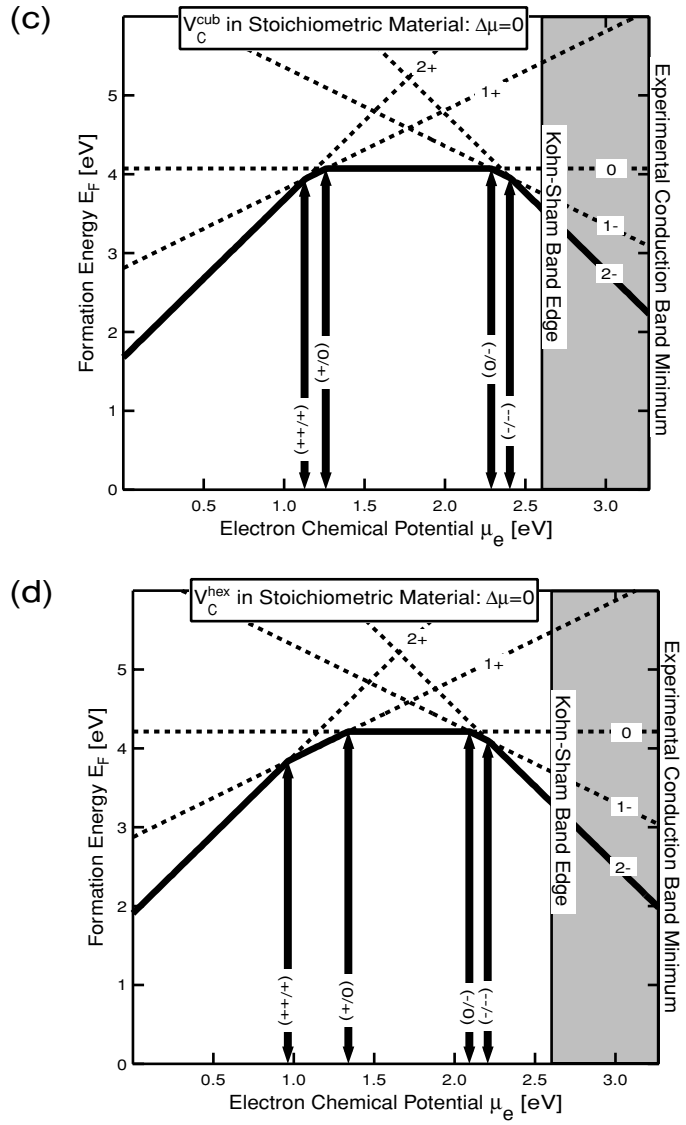

Figure 5. *Continued*

4.5. Carbon vacancy—relaxations

The relaxations around the carbon vacancy in SiC are quite similar to those observed for the silicon vacancy in bulk Si. The strong relaxations in the case of the carbon vacancy in SiC are explained by the following one-electron model: the sp^3 orbital becomes energetically unfavourable and the atoms surrounding the vacancy are likely to relax into a configuration where two pairs of dangling bonds overlap. This Jahn–Teller distortion breaks the symmetry of the molecular sp^3 orbital and—in terms of the one-electron model—the degeneracy of the t_2 orbital is split.

In SiC the four nearest-neighbour atoms of a carbon vacancy build a tetrahedron (see figure 6). To characterize the relaxations around carbon vacancies, we compare the distances

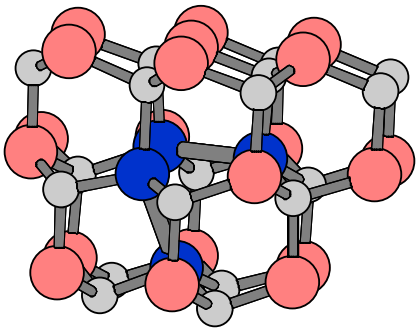

Figure 6. Relaxed atomic positions for the carbon monovacancy at the cubic lattice site V_C^0: the silicon atoms are the bigger, dark grey ones, while C atoms are light grey. The four large, black atoms (Si) are the nearest neighbours to the missing C atoms. For the NN Si atoms one observes an inward relaxation resulting in a Jahn–Teller distortion. The reason for the inward movement is the formation of two new bonds (thick) between each pair of the NN Si atoms to the C vacancy, and hence an energy gain.

(This figure is in colour only in the electronic version)

along the tetrahedra of NN silicon atoms, surrounding the C vacancy, to their ideal distances in a perfect 4H-SiC crystal (cf. the discussion in section 4.3). In table 9 we give the changes of the distances of the NN Si atoms belonging to the tetrahedron around the C vacancy from their ideal distances in 4H-SiC bulk. A strong inwards Jahn–Teller distortion with D_{2d} or D_{3d} point symmetry group is found for both negative ($2-$, $1-$) and neutral charge states. In contrast, for the positive charge states V_C^{1+} and V_C^{2+} an outward relaxation accompanied by a higher symmetry ($\sim C_{3v}$) is found. The volume of the tetrahedron changes for the positive charge states by between +5 and +20% (see table 9). The corresponding volume changes for the neutral and negative vacancies are between -10 and -30% (see table 9).

4.6. Antisites—ionization levels

Without applying the Madelung correction, we find in 4H-SiC four possible ionization levels for the silicon antisite from 4+ up to the neutral defect (figure 7). However, when the formation energies are corrected with the Madelung term, the high-charge states vanish to the valence band, and only the singly positive Si_C^+ and the neutral charge state Si_C^0 are stable. The ionization level $(+/0)$ is then found for Si_C^{cub} at 0.21 eV above the VBM, while for the hexagonal antisite Si_C^{hex} it is located slightly higher at 0.24 eV. Comparing the results in 4H-SiC to other polytypes [29] (2H and 3C), we find only minor differences regarding the positions of the ionization levels (see table 10 and [29]).

4.7. Antisites—relaxations

The atomic relaxations around the carbon antisite C_{Si}^0 are generally inward: the C–C bond lengths are between 10 and 12% shorter than the ideal Si–C bond length (see table 11). For the silicon antisite Si_C, the relaxations are outward, between 13 and 20%. Both neutral antisites exhibit T_d symmetry. In the case of the silicon antisite, the symmetry for higher charge states is broken and a Jahn–Teller distortion with $\sim C_{3v}$ symmetry is found.

According to these results the carbon antisite C_{Si}^0 is both optically and electrically inactive, while the silicon antisite Si_C^+ should be observable (see the discussion in section 5).

Table 9. V_C^{cub} and V_C^{hex}: carbon vacancies at cubic and hexagonal lattice sites in 4H-SiC. Relaxations around a vacancy depend on its charge and spin state. They are given in % compared to the ideal tetrahedral distance between NN silicon atoms. The distances b_1–b_6 are labelled according to figure 3. The last two columns give the tetrahedral volume change $\Delta V = 100(V - V_0)/V_0$ and the symmetry groups for the defects.

	Tetrahedral distances (%) compared to ideal distance							
Charge	b_1	b_2	b_3	b_4	b_5	b_6	ΔV	Symmetry
Carbon vacancy—cubic site: V_C^{cub}								
2+	+7.6	+7.5	+5.6	+7.8	+5.7	+5.6	+21%	C_{3v}
1+	−2.3	+3.8	+2.6	+4.7	+3.5	−1.6	+5%	$\sim C_{2v}$
0	−12.1	+1.3	+0.2	+2.1	+1.2	−10.5	−12%	$\sim D_{2d}$
1−	−18.4	+0.9	−7.6	+0.9	−6.8	−1.7	−18%	
2−	−15.6	−5.3	−0.5	−4.9	−1.1	−3.4	−28%	
Carbon vacancy—hexagonal site: V_C^{hex}								
2+	+5.2	+5.5	+5.5	+6.6	+6.4	+6.7	+19%	C_{3v}
1+	+2.2	+2.4	+2.4	+5.4	+5.3	+5.3	+12%	C_{3v}
0	−10.0	+0.4	−0.6	+3.2	+2.4	−8.6	−9%	$\sim D_{2d}$
1−	−10.1	+0.8	−11.2	+2.8	−4.9	+2.4	−11%	
2−	−17.0	−17.9	−0.2	−17.7	+0.5	+0.6	−23%	D_{3d}

Table 10. Si_C: ionization levels for the relaxed silicon antisites in 3C- and 4H-SiC. The results are from LSDA calculations, given in eV above the valence band maximum. The electrostatic interactions between charged supercells are taken into account in the latter values using the Madelung correction. These results indicate that higher charge states (2+, 3+, 4+) do not stabilize.

	Ionization levels (eV above the VBM)				
Si_C	4+/3+	3+/2+	2+/1+	1+/0	
4H cubic	0.19	0.22	0.28	0.40	This work
4H hexagonal	0.20	0.24	0.30	0.43	This work
3C cubic	0.23	0.24	0.37	0.42	Reference [29]
Madelung correction applied					
4H cubic	(−1.12)	(−0.71)	(−0.28)	0.21	This work
4H hexagonal	(−1.11)	(−0.69)	(−0.26)	0.24	This work

5. Discussion

In this section we first try to characterize all intrinsic point defects in 4H-SiC by giving their wanted poster in terms of their properties arising from our calculations: formation energies, symmetries (relaxations), and ionization levels. If not otherwise stated, all cases of charged defects discussed in this section refer to results including the Madelung correction (see section 2.2 and below). In the second part of the discussion we relate the calculated properties to experimental results.

5.1. Properties

5.1.1. Formation energies. The calculated formation energies can give hints as to which kinds of intrinsic point defects tend to dominate under certain growth conditions (C- or

Table 11. Calculated NN distances for all possible antisites in 4H-SiC: C_{Si}^{cub}, C_{Si}^{hex}, Si_{C}^{cub}, and Si_{C}^{hex}. The carbon antisite exists only in the neutral charge state. The numbers a_1–a_4 give the changes in % of the ideal bond length (three bonds 1.862 Å and one 1.871 Å) in 4C-SiC.

		Nearest-neighbour distances (%)				
Defect	Charge	a_1	a_2	a_3	a_4	Symmetry
Carbon antisite in 4H-SiC						
C_{Si}^{cub}	0	−12.0	−11.6	−11.5	−11.6	T_d
C_{Si}^{hex}	0	−10.7	−11.8	−11.4	−11.4	$\sim T_d$
Silicon antisite in 4H-SiC						
Si_{C}^{cub}	0	+13.3	+14.4	+14.1	+14.2	$\sim T_d$
Si_{C}^{hex}	0	+15.0	+14.1	+13.9	+14.0	$\sim T_d$
Si_{C}^{cub}	1+	+13.6	+14.6	+16.2	+16.5	$\sim C_{3v}$
Si_{C}^{hex}	1+	+15.1	+14.5	+16.4	+16.0	$\sim C_{3v}$
Si_{C}^{cub}	2+	+13.7	+15.2	+16.2	+19.5	$\sim C_{3v}$
Si_{C}^{hex}	2+	+15.1	+14.8	+18.5	+17.3	$\sim C_{3v}$
Si_{C}^{cub}	3+	+13.8	+16.7	+17.4	+19.0	$\sim C_{3v}$
Si_{C}^{hex}	3+	+15.1	+16.7	+17.7	+18.7	$\sim C_{3v}$
Si_{C}^{cub}	4+	+13.9	+18.4	+18.1	+18.5	C_{3v}
Si_{C}^{hex}	4+	+15.1	+18.0	+18.6	+18.5	C_{3v}

Si-rich, n- or p-type-doped). The effect of stoichiometry is generally small: for vacancies the formation energies may vary by ±0.33 eV over the whole range of the atomic chemical potential difference. For antisites the corresponding value is ±0.66 eV. The influence of doping turns out to be more important, favouring either positive or negative charge states (cf. section 2.2). We note generally small differences in the formation energies for different (cubic or hexagonal) lattice sites of the order of 0.1 eV.

5.1.2. Symmetries (relaxations). The relaxations around the various intrinsic point defects have been given in the tables in sections 4.3, 4.5, and 4.7. There also the corresponding symmetry groups have been indicated. Information derived from magnetic resonance methods (EPR, ODMR, ENDOR, . . .) can make it possible to attribute a symmetry group to certain defects.

5.1.3. Ionization levels. The ionization levels have been calculated as the intersection points of the corresponding formation energy curves for differently charged defects. Generally, one notes a slight site dependence of the ionization levels around 0.01–0.2 eV. In sections 4.1 and 4.4 we indicated both the Kohn–Sham band edge and the experimental conduction band minimum in the figures given there. To directly compare our results to those of Zywietz *et al* [27], we shifted the ionization levels (E'_D) in a similar manner for negative charge states upwards, and thus obtained higher values for negative charge states just as in those calculations—given in table 3 in parentheses.

To correct for the electrostatic self-interaction arising from charged supercells, we employed the Madelung correction, in order to better compare calculated ionization levels to experimental ones (see figures 8(a) and 8(b) for the level scheme without and with Madelung correction). Nevertheless, it is difficult to conclusively identify experimentally detected ionization levels and attribute them to a certain defect. The main experimental techniques are

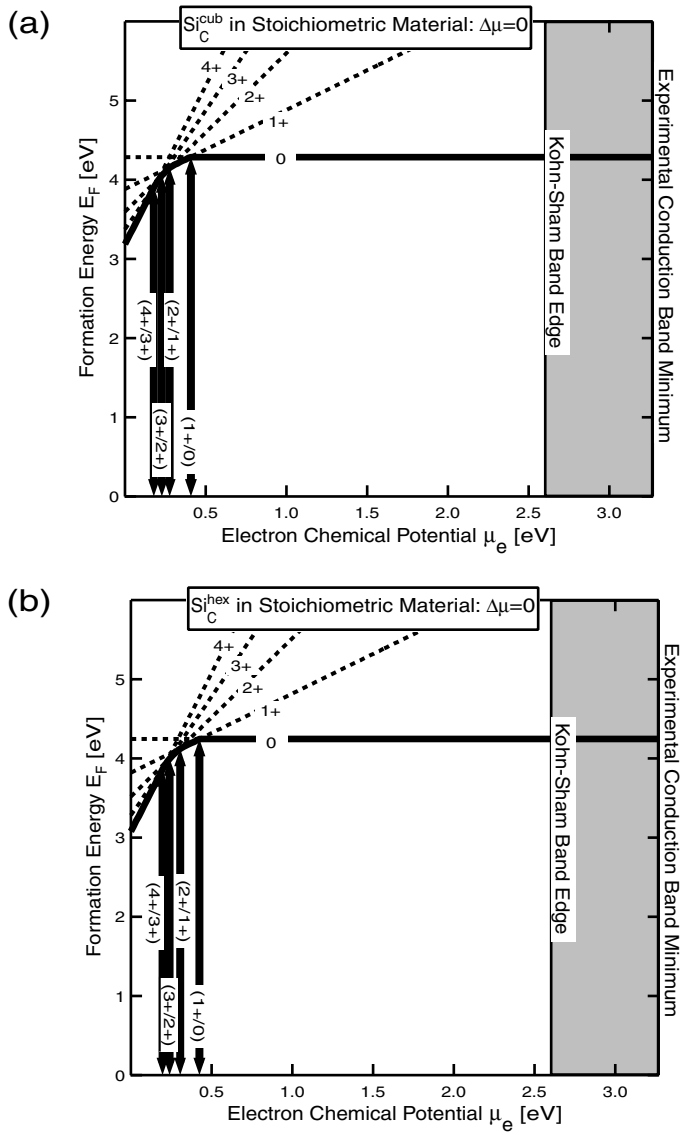

Figure 7. Silicon antisites on cubic ((a) and (c)) and hexagonal ((b) and (d)) lattice sites for stoichiometric material. Panels (a) and (b) ignore the Madelung correction, while lower panels (c) and (d) include it. Formation energies for different charge states (dashed lines), with each charge state indicated, are given. The thick solid line corresponds to the lowest formation energy as a function of the electron chemical potential. The ionization levels (indicated by arrows) are at the intersections of the dashed lines. Note that the highly positive charge states are shifted close to or into the valence band when the Madelung correction is applied.

photoluminescence and capacitance transient methods (PL, DLTS). Also positron annihilation spectroscopy (PAS) has been used to study optical transitions, and thus to determine the ionization levels. Generally, it is very difficult to attribute ionization levels determined by DLTS to microscopically identified defects. One way is to carefully compare the annealing behaviour of deep-level defects with those of known EPR centres after irradiation damage.

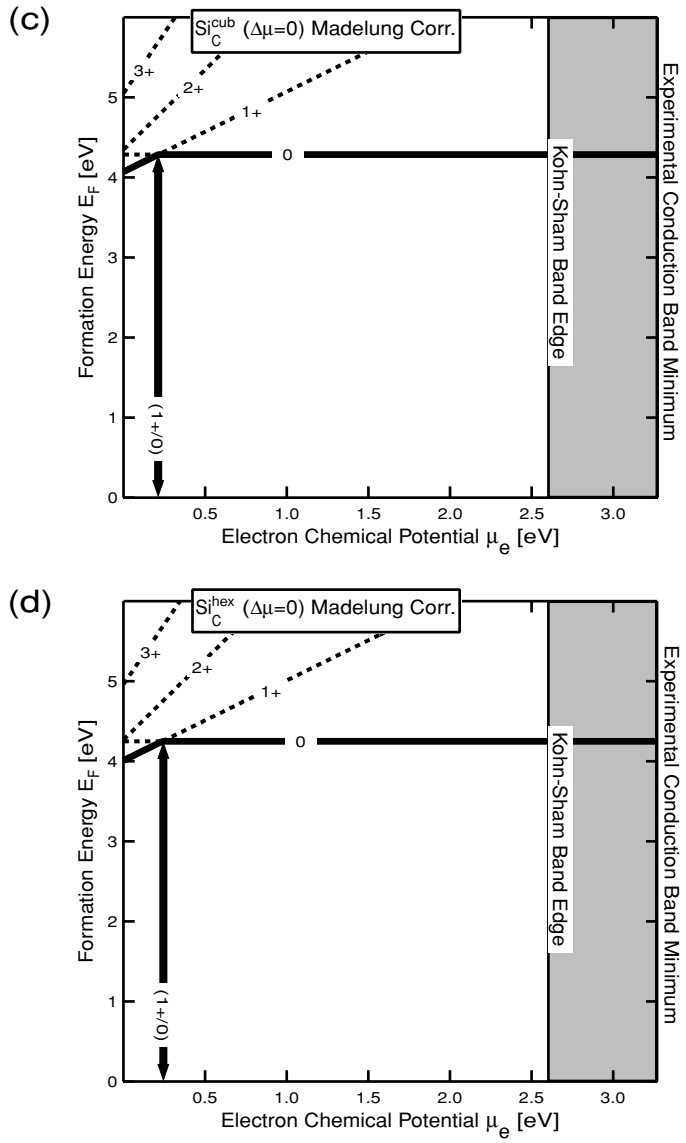

Figure 7. *Continued*

5.2. Silicon vacancies

A characteristic for silicon vacancies in SiC is their high formation energy of about 8 eV (neutral vacancy in stoichiometric material). All other intrinsic point defects in SiC have a formation energy of about 4 eV. Only for highly n-type materials may negatively charged Si vacancies also have formation energies in that range. Despite their large formation energy, Si vacancies are found not only as irradiation defects but also in as-grown SiC [52].

The electronic structure of the silicon vacancy in SiC resembles that of the monovacancy in bulk diamond—the local atomic environments are identical. As in the case of diamond, V_{Si}^{-} and V_{Si}^{0} are found in high-spin states, exhibiting a large outward breathing relaxation

of the surrounding C atoms, and preserving approximately the T_d symmetry of the crystal, while for the positive charge state V_{Si}^{+} the symmetry is lowered to C_{3v} (deviations have been indicated in the tables of section 4.3). The reason for the outward relaxation of the surrounding carbon atoms seems to be that they cannot form any new bonds (energy lowering) by inward relaxation, since the C–C bond length in diamond bulk is 1.541 Å and in graphite 1.426 Å, and is hence too short. Hence, NN carbon atoms undergo a rehybridization, relax outward, and form more planar sp^2 graphite-like bonds leaving a π-dangling bond, which is lower in energy than a σ-dangling bond [53]. For 2−, 1−, and the neutral charge state the high-spin states ($S = 1, 3/2, 1$) give rise to the lowest total energies. Experimentally, the high-spin state ($S = 3/2$) for V_{Si}^{-} has been observed in 4H-SiC [13]. Also for the neutral vacancy there are experimental indications for a high-spin state [10].

The ionization levels are found for the $(-/0)$ transition in the lower half of the band gap ($E_V + 0.57$ eV and $E_V + 0.64$ eV for cubic and hexagonal lattice sites, respectively), while the $(2-/-)$ and the $(3-/2-)$ levels are in the upper half of the band gap, at about $E_V + 1.6$ eV and $E_V + 2.2$ eV, respectively (see figure 8). The possibility that in highly p-type material silicon vacancies can exist in the positive charge state depends on the positions of the acceptor levels, which fixes the electron chemical potential above the valence band for high-doping conditions.

For 3C-SiC the ionization level $(-/0)$ has been found in *ab initio* calculations at about $E_V + 0.45$ eV [54], which is in good agreement with estimations based on PL data giving $E_V + 0.5$ eV [3, 4]. Hence, we may expect to find the $(-/0)$ ionization level even for 4H-SiC in that range, which agrees well with our results. This is also supported by the fact that silicon vacancies in the negative charge state are found in both p- and n-type 3C-SiC [4], which in turn implies that the $(-/0)$ level must be situated in the lower half of the band gap. This and our results agree with combined PL and ODMR studies where it has been estimated that the position of the $(-/0)$ level is at least 1.8 eV below the CBM and that the $(3-/2-)$ level should be closely below the n-donor level [10]. Since DLTS studies on acceptor-like deep levels are rare, only a few levels have been identified so far: due to its similar annealing behaviour compared with V_{Si} found by PAS and the T1-EPR centre, the H1 level, found at $E_V + 0.55$ eV in 6H-SiC [55], can be attributed to the $(-/0)$ level of the silicon vacancy. This is close to our results of $E_V + 0.57$ eV and $E_V + 0.64$ eV for cubic and hexagonal sites, respectively (see figure 8).

A combined PAS-EPR study [16] identified the positron lifetime signal from silicon vacancies with the T1-EPR centre (V_{Si}^{-}) on the basis of their identical annealing behaviour. Combining this with recent theoretical calculations for the annihilation characteristics of vacancies at silicon and carbon sites [56] makes an unambiguous identification of the positron lifetime signal related to V_{Si} possible. Hence, IR absorption, changing the positron trapping rate into V_{Si} due to changes in their charge state, clearly identified the ionization levels of the silicon vacancy at $E_C - 0.6$ eV and $E_C - 1.1$ eV in 6H-SiC [57]. This again fits well with our results giving the $(3-/2-)$ and the $(2-/1-)$ levels at $E_V + 2.14$ eV ($E_V + 2.26$ eV) and $E_V + 1.60$ eV ($E_V + 1.58$ eV) for cubic (hexagonal) sites, respectively (see figure 8(b)). These values are at $E_{KS} - 0.5$ eV and $E_{KS} - 1.0$ eV below the Kohn–Sham band edge. DLTS indicates a double level at $E_C - 0.62$ eV and $E_C - 0.64$ eV for electron-irradiated n-type 6H-SiC [22], which shows the same annealing behaviour as the T1-EPR centre and PAS [4, 16]. A similar level at $E_C - 0.68$ eV was also found for 4H-SiC [58], but no annealing study was performed there.

After electron irradiation of 4H-SiC a level denoted as EH5 ($E_C - 1.13$ eV) was found [58]. One at a corresponding energy was detected after a similar irradiation treatment in 6H-SiC: E7 ($E_C - 1.25$ eV) [59]. Since they are both acceptor-like [58, 59] they may

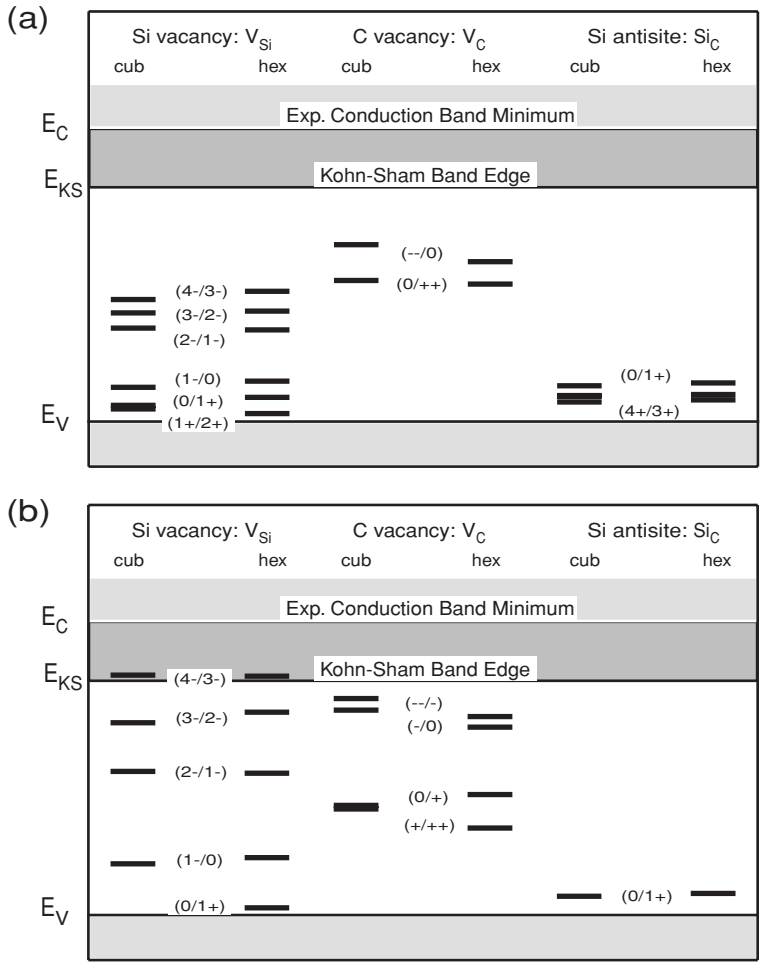

Figure 8. Energy-level schemes for Si and C vacancies as well as for Si antisites (C antisites do not have any ionization levels) without (a) and with (b) Madelung correction. The results are given for both cubic and hexagonal lattice sites, obtained from LSDA calculations employing a 128-atom supercell. Highly positively charged states are shifted by the Madelung correction into the valence band and highly negative charge states into the upper half of the band gap or into the conduction band (b).

be candidates for being the $(2-/-)$ level, even though their annealing behaviour is not clear so far.

5.3. Carbon vacancies

The carbon vacancy in its neutral charge state is characterized in stoichiometric material by a formation energy of about 4 eV. For highly p- or n-type material the formation energy may drop to about 2 eV for both doubly positive or doubly negative charge states.

The electronic structure of the carbon vacancy in SiC resembles that of the monovacancy in pure silicon, since the local atomic environment is the same. About 30% of the electronic wave function is located at the nearest-neighbour silicon atoms adjacent to the vacancy, while

the rest of the wave function is spread out over more distant neighbours. In contrast to the case for pure silicon, the four dangling bonds directed towards the next-nearest neighbours of the vacancy hybridize in different ways depending on its charge state. Hence, the relaxation is also affected. Carbon vacancies in neutral or negative charge states are characterized by large Jahn–Teller-distorted inward relaxations, resulting in breaking of the T_d symmetry towards D_{2d}, as already noticed in [27].

The reason for this behaviour is an energy lowering by the formation two new bonds of the nearest-neighbour Si atoms. This re-binding of the dangling bonds is only possible by an inward relaxation bringing the Si–Si distances to about 2.70 Å and, hence, closer to the bond length in Si bulk (2.35 Å). For the lattice this is, even with the cost of lattice distortion, the energetically most favourable way to deal with dangling bonds [53]. Similar features have been observed for the Si monovacancy in Si bulk, where the distance for the new bonds is about 2.65 Å. For the doubly positive charge state we find for both cubic and hexagonal lattice sites outward relaxations, which nearly preserve the T_d symmetry. For the singly negative charge state a significant difference between C vacancies at cubic or hexagonal sites appears.

That positively charged carbon vacancies are found only in p-type material is reasonable, since we find the ionization levels for $(+/2+)$ and $(0/+)$ slightly below the mid-gap, while the others ($(-/0)$ and $(2-/-)$) are about $E_{KS} - 0.3$ eV and $E_{KS} - 0.2$ eV below the Kohn–Sham band edge for V_C^{hex}. For V_C^{cub} the levels are located at $E_{KS} - 0.5$ eV and $E_{KS} - 0.4$ eV (see figure 8(b)). Note that the Madelung correction employed has removed the otherwise found negative-U behaviour [27]. This is reasonable since, to our knowledge, no negative-U behaviour has been found experimentally for $(2-/0)$ or $(0/2+)$. Without the Madelung correction our results agree very well with those of reference [27].

A convincing identification of the microscopic structure of the carbon vacancy in SiC has only been achieved for the positive charge state V_C^+ in irradiation-damaged p-type 3C-SiC (T5 centre) [3] or p-type 4H- and 6H-SiC (EI5 centre) [11]. The identification is based on an analysis of first- and second-nearest-neighbour hyperfine interactions directly resolved in the EPR spectra. Like for the silicon vacancy V_{Si}^-, V_C^+ also does not show any site dependence for the EPR spectra in 4H or 6H polytypes [11]. The annealing behaviour is characterized by one sharp annealing stage at about 200°C in 3C-SiC [3, 4], while it may be slightly higher in 4H- and 6H-SiC [11]. The symmetry C_{3v}, determined for 4H- and 6H-SiC [11], is in good agreement with our findings (compare table 9).

Since the zero-to-negative ionization levels of the carbon vacancy are situated close to the conduction band, there are several candidate levels from DLTS studies. The only convincingly identified level is Ei ($E_C - 0.51$ eV) in 6H-SiC [22], since it shows the same annealing behaviour as the T5 EPR centre (V_C^+). This level has also been found in 6H with a similar annealing behaviour to V_C [59]. But since Ei cannot be the carbon vacancy in its positive charge state, we believe instead that Ei is related to the $(2-/-)$ or $(-/0)$ charge transition of the carbon vacancy (compare figure 8(b)). Ei in 6H may correspond to EH1 ($E_C - 0.45$ eV) found in 4H-SiC [58].

The other ionization levels of the carbon vacancy are with one exception (V_C on a hexagonal site: $(+/2+)$ at $E_V + 0.97$ eV) near the mid-gap and hence difficult to access with DLTS. One level, H2 ($E_V + 0.78$ eV), showing an annealing behaviour as expected for carbon vacancies has been found in electron-irradiated p-type 6H-SiC [55]. Hence, H2 may well be associated with the $(+/2+)$ ionization level of the carbon vacancy on a hexagonal site.

The EH6/EH7 level ($E_C - 1.65$ eV) [58] would be at the right position for ionization levels of the carbon vacancy. But it persists to much higher temperatures and, hence, may obscure the observation of the ionization levels of V_C situated around the mid-gap.

5.4. Antisite defects

Of all simple point defects the neutral carbon antisite C_{Si} has the lowest formation energy, of about 3.5 eV, in stoichiometric material. Its counterpart, the silicon antisite Si_C, has a higher formation enthalpy of 4.3 eV under the same conditions.

The C_{Si} antisite, which exists according to our calculations only in the charge-neutral state, shows strong inward relaxations of the surrounding Si atoms while preserving the T_d symmetry (see table 11). The silicon antisite Si_C, on the other hand, shows strong outward relaxation of the surrounding C atoms. Even here the T_d symmetry prevails for the charge-neutral state, but is broken for the positively charged state (see table 11).

Since the carbon antisite C_{Si} is found only in the charge-neutral state, no ionization levels exist. Employing the Madelung correction, only the (+/0) level is stable at $E_V + 0.21$ eV and $E_V + 0.24$ eV for the silicon antisite Si_C on cubic and hexagonal lattice sites, respectively. This means that Si_C should act as a shallow donor in highly p-type material.

Even though the carbon antisite C_{Si} has the lowest formation energy of all intrinsic simple point defects considered, it turns out difficult to prove its presence by nearly all experimental methods. It does not have an unpaired electron (it is not EPR active) nor does it exist in charge states other than neutral (no DLTS or PL possible), nor can it be proved to be a shallow positron trap. The only possible way to detect it may be by its induced lattice distortions via channelling techniques. Since the silicon antisite Si_C has an ionization level close to the valence band it may be detected by capacitance transient techniques.

The EI6 EPR centre has been recently identified in electron-irradiated p-type 4H- and 6H-SiC as the isolated Si antisite in the positive charge state Si_C^+, since it was only found in p-type material [11]. The identification is based on hyperfine interactions. The defect is supposed to have spin 1/2 and C_{3v} symmetry. This coincides with our findings for that defect.

Only one candidate level, HH1 in electron-irradiated p-type 6H-SiC, has been found in a recent investigation on electron-irradiated material at $E_V + 0.35$ eV [58]—not far from our calculated value. However, it appeared only after annealing at about 350°C and, hence, is likely to be a complex. On the other hand, there exist older results for neutron-irradiated 3C-SiC epitaxial layers, where three levels above the VBM have been detected: H1 ($E_V + 0.18$ eV), H2 ($E_V + 0.24$ eV), and H3 ($E_V + 0.51$ eV) [19, 60]. All defects should anneal at about 350°C. In principle H1 and H2 could be due to antisite defects as calculated by us. But a convincing identification would only be possible if one could compare the annealing behaviour of H1 and H2 with the recently discovered EPR centre EI6 identified as Si_C^+ [11].

5.5. Other polytypes

In [30] we performed calculations for the silicon vacancy in 2H-SiC. Comparing these to the results for 4H-SiC, we see only minor differences between these polytypes. We can even note that the hexagonal-site silicon vacancies have nearly the same formation energies of 8.1 eV under stoichiometric conditions. The formation energy of the silicon vacancy in 4H at the cubic site is about 0.1 eV lower. Comparing our results for a 128-atom rectangular supercell to a calculation for 3C-SiC [27] employing a 216-atom cubic supercell, we find them close to identical. But large differences are found when using for 3C only 128-atom supercells, indicating that the use of a 128-atom cubic supercell and only the Γ point does not give converged results for 3C-SiC.

6. Conclusions

We find for the neutral antisite defects and for the neutral carbon vacancy low formation energies around 3–4 eV. This indicates that their concentration as grown-in defects could be high in SiC, which has also been claimed in the experimental literature. For the neutral silicon vacancy, the formation energy is found to be as high as 8 eV. The results for the formation energy vary to some extent (0.03–0.14 eV) depending on the lattice site, with the cubic case generally favoured. In comparison with those for other polytypes the results are found to be qualitatively similar.

The silicon vacancy V_{Si} has one ionization level $(0/+)$ very close to the valence band maximum. Hence, it may be—dependent on the position of the donor level—difficult to observe. The level $(-/0)$ is found at about $E_V + 0.5$ eV. The other two levels are situated above the middle of the band gap. All are in reasonable agreement with positions determined experimentally. We realize that the monovacancy in diamond is physically similar to the silicon vacancy in SiC. Both exhibit the high-spin ground state and an undistorted T_d symmetry, which is found experimentally by means of EPR.

For the carbon vacancy V_C, we find four stable charge states ranging from $2+$ to $2-$, where the positive ones are slightly below the mid-gap and the negative ones are close to the conduction band. Applying the Madelung correction, which takes into account the spurious electrostatic interactions between charged supercells, the singly negative and positive charge states stabilize as well. Thus, we do not find the previously claimed negative-U transitions $(2+/0)$ and $(0/2-)$ [27]. In fact, experimentally the carbon vacancy has been recently found to be stable in the positive charge state V_C^+ in 4H- and 6H-SiC [11]. Also for the carbon vacancy, the calculated levels are in reasonable agreement with experiment.

The antisite defects Si_C and C_{Si} are generally found to be inactive both electrically and optically. However, the positive ionization levels of Si_C can be found when the electron chemical potential is low, below 0.24 eV above the VBM. While levels near this position have been found, their origin remains unclear.

Depending on the charge state, the relaxation symmetries for V_{Si} are C_{3v} and T_d. For V_C a strong Jahn–Teller distortion, with the symmetry group $\sim D_2$, is found in most charge states. C_{Si} remains undistorted, while for Si_C, in general, the C_{3v} symmetry is obtained. The carbon vacancy V_C^+ and the silicon antisite Si_C have recently been found in 4H- and 6H-SiC to exhibit the same symmetries as those calculated here [11].

Acknowledgments

The authors wish to express their thanks for the generous provision of computing resources at the Centre of Scientific Computing (CSC) in Espoo, Finland, and at the National Supercomputer Centre (NSC) in Linköping, Sweden. We wish to thank all the members of the Materials Physics Group at Linköping University for useful discussions. This work was supported by the Academy of Finland through its Centres of Excellence Programme 2000–2005.

TEMS acknowledges the support of a Marie-Curie Grant from the European Commission.

References

[1] Käckell P, Wenzien B and Bechstedt F 1994 *Phys. Rev.* B **50** 17037

[2] Rauls E, Lingner Th, Hajnal Z, Greulich-Weber S, Frauenheim Th and Spaeth J M 2000 *Phys. Status Solidi* b **217** R1

[3] Itoh H, Yoshikawa M, Nashiyama I, Misawa S, Okumura H and Yoshida S 1992 *J. Electron. Mater.* **21** 707
[4] Itoh H, Kawasuso A, Ohshima T, Yoshikawa M, Nashiyama I, Tanigawa S, Misawa S, Okumura H and Yoshida S 1997 *Phys. Status Solidi* b **162** 173
[5] Egilsson T, Henry A, Evanov I G, Lindström J L and Janzén E 1999 *Phys. Rev.* B **59** 8008
[6] Egilsson T, Bergman J P, Evanov I G, Henry A and Janzén E 1999 *Phys. Rev.* B **59** 1956
[7] Egilsson T 1999 Bound excitons in silicon carbide *Dissertation* No 588 (Sweden: Linköping University)
[8] Son N T, Sörman E, Chen W M, Singh M, Hallin C, Kordina O, Monemar B and Janzén E 1996 *J. Appl. Phys.* **79** 3784
[9] Son N T, Sörman E, Chen W M, Hallin C, Kordina O, Monemar B and Janzén E 1997 *Phys. Rev.* B **55** 2863
[10] Sörman E, Son N T, Chen W M, Kordina O, Hallin C and Janzén E 2000 *Phys. Rev.* B **61** 2613
[11] Son N T, Hai P N and Janzén E 2001 *Mater. Sci. Forum* **353–356** 499
[12] Bardeleben H J von, Cantin J L, Henry L and Barthe M F 2000 *Phys. Rev.* B **62** 10841
[13] Wimbauer T, Meyer B K, Hofstaetter A, Scharmann A and Overhof H 1997 *Phys. Rev.* **56** 7384
[14] Kawasuso A, Itoh H, Okada S and Okumura H 1996 *J. Appl. Phys.* **80** 5639
[15] Brauer G, Anwand W, Coleman P G, Knights A P, Plazaola F, Pacaud Y, Skorupa W, Störmer J and Willutzki P 1996 *Phys. Rev.* B **54** 3084
[16] Kawasuso A, Itoh H, Morishita N, Yoshikawa M, Ohshima T, Nashiyama I, Okada S, Okumura H and Yoshida S 1998 *Appl. Phys.* A **67** 209
[17] Polity A, Huth S and Lausmann M 1999 *Phys. Rev.* B **59** 10603
[18] Ling C C, Beling C D and Fung S 2000 *Phys. Rev.* B **61** 8016
[19] Nagesh V, Farmer J W, Davis R and Kong H S 1987 *Appl. Phys. Lett.* **50** 1138
[20] Hemmingsson C G, Son N T, Ellison A, Zhang J and Janzén E 1998 *Phys. Rev.* B **58** R10119
[21] Hemmingsson C G, Son N T, Ellison A, Zhang J and Janzén E 1999 *Phys. Rev.* B **59** 7768 (erratum)
[22] Aboelfotoh M O and Doyle J P 1999 *Phys. Rev.* B **59** 10823
[23] Rempel A A, Müller M A, Reichle K, Sprengel W, Major J and Schaefer H-E 2001 Identification of electron irradiation induced atomic vacancies on the two sublattices of silicon carbide by means of coincident Doppler broadening *Proc. ICPA-12 (München, August 2000); Mater. Sci. Forum* **363–365** 70–72
[24] Li Y and Lin-Chung P J 1987 *Phys. Rev.* B **36** 1130
[25] Talwar D N and Feng Z C 1991 *Phys. Rev.* B **44** 3191
[26] Wang C, Bernholc J and Davis R F 1988 *Phys. Rev.* B **38** 12752
[27] Zywietz A, Furthmüller J and Bechstedt F 1999 *Phys. Rev.* B **59** 15166
[28] Zywietz A, Furthmüller J and Bechstedt F 2000 *Phys. Rev.* B **62** 6854
[29] Torpo L, Pöykkö S and Nieminen R M 1998 *Phys. Rev.* B **57** 6243
[30] Torpo L M, Nieminen R M, Laasonen K E and Pöykkö S 1999 *Appl. Phys. Lett* **74** 221
[31] Torpo L and Nieminen R M 1999 *J. Mater. Sci. Eng.* B **61–62** 593
[32] Makov G and Payne M C 1995 *Phys. Rev.* B **51** 4014
[33] Ceperley D M and Alder B J 1980 *Phys. Rev. Lett.* **45** 566
[34] Perdew J and Zunger A 1981 *Phys. Rev.* B **23** 5048
[35] Vosko S H, Wilk L and Nusair M 1980 *Can. J. Phys* **58** 1200
[36] Bachelet G B, Hamann D R and Schlüter M 1982 *Phys. Rev.* B **26** 4199
[37] Vanderbilt D 1990 *Phys. Rev.* B **41** 7892
[38] Laasonen K, Pasquarello A, Car R, Lee C and Vanderbilt D 1993 *Phys. Rev.* B **47** 10142
[39] Press W H, Teukolsky S A, Vetterling W T and Flannery B P 1992 *Numerical Recipes* 1st edn (Cambridge: Cambridge University Press)
[40] Tassone F, Mauri F and Car R 1994 *Phys. Rev.* B **50** 10561
[41] Williams A and Soler J 1952 *Bull. Am. Phys. Soc.* **32** 409
[42] Pöykkö S, Puska M J and Nieminen R M 1998 *Phys. Rev.* B **57** 12174
[43] Murnaghan F D 1994 *Proc. Natl Acad. Sci. USA* **30** 244
[44] *Landolt–Börnstein New Series* 1989 ed O Madelung and M Schulz (Berlin: Springer)
[45] Zhang S B and Northrup J E 1991 *Phys. Rev. Lett.* **67** 2339
[46] Lento J, Pesola M, Mozos J-L and Nieminen R M 2000 *Appl. Phys. Lett.* **77** 232
[47] Stoneham A M 1975 *Theory of Defects in Solids* (Oxford: Oxford University Press)

[48] Watkins G D 1986 The lattice vacancy in silicon *Deep Centers in Semiconductors* ed S T Pantelides (New York: Gordon and Breach) pp 147–83
[49] Watkins G D and Corbett J W 1964 *Phys. Rev.* **134** A1359
[50] Isoya J, Kanda H, Uchida Y, Lawson S C, Yamasaki S, Itoh H and Morita Y 1992 *Phys. Rev.* B **45** 1436
[51] Deák P, Miró J, Gali A, Udvardi L and Overhof H 1999 *Appl. Phys. Lett.* **75** 2103
[52] Ling C C, Deng A H, Fung S and Beling C D 2000 *Appl. Phys.* A **70** 33
[53] Lannoo M *Mater. Sci. Eng.* B **22** 1
[54] Mattausch A, Bockstedte M and Pankratov O 2001 *Mater. Sci. Forum* **353–356** 323
[55] Gong M, Fung S, Beling C D and You Z 1999 *J. Appl. Phys.* **85** 7120
[56] Staab T E M, Torpo L, Puska M J and Nieminen R M 2001 *Mater. Sci. Forum* **353–356** 533
[57] Arpiainen S, Saarinen K, Henry L and Barthe M-F 2001 to be published
[58] Hemmingsson C, Son N T, Kordina O, Bergman J P, Janzén E, Lindström J L, Savage S and Nordell N 1997 *J. Appl. Phys.* **81** 6155
[59] Hemmingsson C, Son N T, Kordina O and Janzén E 1998 *J. Appl. Phys.* **84** 704
[60] Nagesh V, Farmer J W, Davis R F and Kong H S 1990 *Radiat. Eff. Defects Solids* **112** 77